

**INNOVATIVE EXPERIMENTAL PARTICLE PHYSICS
THROUGH TECHNOLOGICAL ADVANCES –
PAST, PRESENT AND FUTURE**

H. W. K. CHEUNG

*Fermi National Accelerator Laboratory,
P.O. Box 500,
Batavia, IL 60510-0500, USA
E-mail: cheung@fnal.gov*

This mini-course gives an introduction to the techniques used in experimental particle physics with an emphasis on the impact of technological advances. The basic detector types and particle accelerator facilities will be briefly covered with examples of their use and with comparisons. The mini-course ends with what can be expected in the near future from current technology advances. The mini-course is intended for graduate students and post-docs and as an introduction to experimental techniques for theorists.

1. Introduction

Despite the fancy title of this mini-course, the intention is to give a brief introduction to experimental particle physics. Since there are already some excellent introductions to this topic and some textbooks that cover various detectors in detail, a more informal approach to the topic is given in this mini-course. Some basic detector elements are covered while reviewing examples of real experiments, and experimental techniques are introduced by comparing competing experiments. Some aspects of experimental design are also briefly reviewed. Hopefully this will provide a more engaging introduction to the subject than a traditional textbook. This short mini-course cannot replace a real experimental physics course; the reader is just given a taste. Unfortunately the lack of space for this writeup means that not even the basic detection methods and detector types can be described. Instead detector types in *italics* will be briefly described in a glossary at the end of this writeup. For further reading, the reader can find the relevant physics of particle interactions and detailed descriptions of many different types of particle detectors in a number of textbooks and articles.¹

Although this mini-course is devoted to the physics impact of some significant technological advances, it should be noted that the improvements in experimental techniques usually progress in steady steps. Quite often advances are linked to steady progress in the following areas:

- Higher energy available or/and higher production rate.
- Improvements in momentum or/and position resolution.
- Better particle identification methods.
- Increase in detector coverage or energy resolution.
- More powerful signal extraction from background.
- Higher accuracy (due to increase in data statistics, reduction of experimental systematic uncertainties, or reduction in theoretical uncertainties).

Discoveries are often made through a series of incremental steps, though of course the discoveries themselves can be in a surprising direction! The topics I have chosen for the two lectures of this mini-course is the discovery and subsequent study of the charm quark, and the future of bottom quark physics. The outlines for the two lectures are illustrated in Fig. 1.

2. Part I: Discovery of Charm

The discovery of the J/ψ meson is well documented by many books and articles² as well as in the Nobel lectures of Ting³ and Richter.⁴ Besides being a great classic story of discovery, we can also use it to illustrate some of the detection techniques and the physics and ideas behind the design of the experiments involved.

2.1. A Missed Opportunity: Resolutions Matter!

Since the leptons, electrons and muons, are basically point-like, stable or long-lived, and interact primarily via the well understood and calculable electroweak force, they have served as the “eyes” in probing many experimental processes. One of those processes under study in the 1970’s was hadron interactions. The interests in this study included the investigation of the electromagnetic structure of hadrons, the study of the then-called “Heavy photons” ρ , ω and ϕ and the search for additional ones, as well as the search for the neutral intermediate vector boson, the Z^0 .

One experiment doing such a study offers a lesson on the importance of experimental resolution. This was an experiment at Brookhaven National Laboratory (BNL) using the Alternating-Gradient Synchrotron

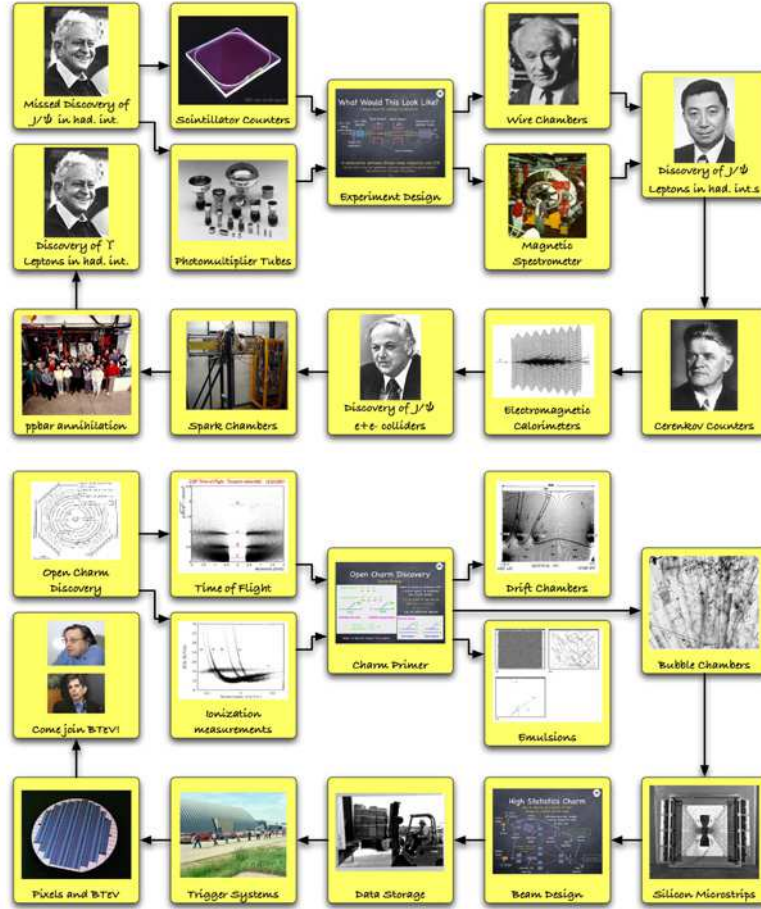


Figure 1. Outline for the the mini-course: (top) lecture 1; (bottom) lecture 2.

(AGS) carried out by Leon Lederman's group. They performed studies of $p + U \rightarrow \mu^+ \mu^- X$ and missed discovering the J/ψ in 1970, four years before the actual discovery.

A diagram showing Lederman's 1970 experiment is given in Fig. 2.^{5,6} The experiment was to study the interaction of the 22-30 GeV proton beam on a Uranium target. The aim was to detect a pair of oppositely charged muons coming from the interaction.

The emphasis of this experiment was to get a clean signature for muons

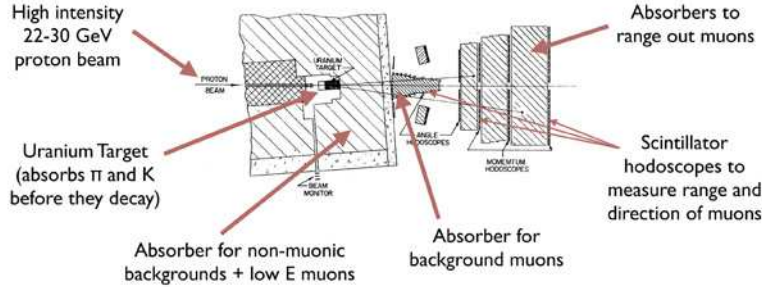


Figure 2. Diagram of the spectrometer for the Lederman 1970 experiment.⁵

directly produced in the target. The main background to eliminate was muons from the decay of pions and kaons. A high atomic number target like Uranium has a short interaction length which serves to both cause a lot of the proton beam to interact and also to absorb pions and kaons produced in the interactions before they can decay. This is followed by additional material to absorb non-muonic backgrounds and low energy muons. Muons from hadron decay typically have lower energy than those directly produced in the primary proton-Uranium interaction. Another specially shaped heavy absorber serves to absorb more background muons while *scintillator hodoscopes* measure the direction of the surviving muons. The final material at the end of the detector serves to measure the range and therefore the energy of the muons.

Although all the absorber material helps to give a much cleaner sample of dimuon events, it also causes a lot of multiple Coulomb scattering (MCS), especially as the material is of high Z and therefore has short radiation length. This large MCS limited the dimuon mass resolution at $3 \text{ GeV}/c^2$ to about $\approx 13\%$, or $\approx 400 \text{ MeV}/c^2$. Even with all the absorber the signal-to-background (S/B) is relatively small. The S/B at low dimuon mass ($\approx 2 \text{ GeV}/c^2$) was about 2%, increasing up to 50% at higher dimuon mass ($\approx 5 \text{ GeV}/c^2$). This means relatively large background subtractions are needed. Another concern was the low acceptance and efficiency at low dimuon mass which therefore needed larger corrections.

The raw and corrected dimuon mass distributions are given in Fig. 3. Although the large background subtraction and the uncertainty in the correction might have contributed to the missed discovery of a peak at the J/ψ mass, if the dimuon mass resolution were sufficiently better, the J/ψ peak would still have been observed. The experimenters did many tests

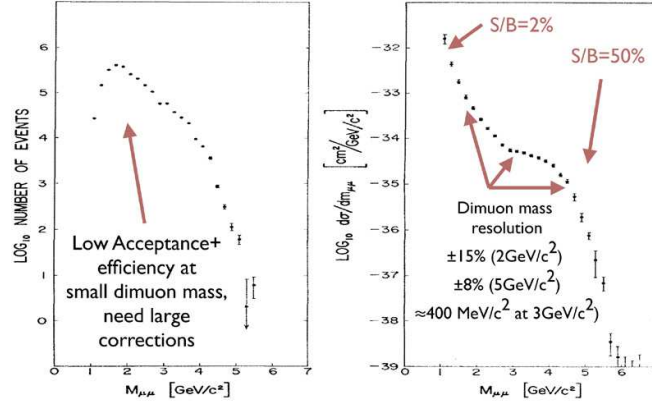


Figure 3. Results for the dimuon mass spectrum from the Lederman 1970 experiment.⁵ (left) raw distribution; (right) corrected spectrum.

and gave limits for a narrow state, but they had to conclude in the end that there was “no forcing evidence of resonant structure.”

2.2. Elements of Experimental Design

With hindsight how would we change Lederman’s 1970 experiment so we could observe the J/ψ ? Instead of leaving it as a task to the reader, it is instructive to go through this in a little detail. The most obvious things to include in a redesign are the following:

- (i) Improve the momentum resolution, which means having less material for MCS, using a magnet for momentum determination and using a finer spatial resolution detector than a scintillator hodoscope.
- (ii) Increase the S/B, which means separating muons better from hadrons and enriching the sample of dimuons *vs.* single muons.
- (iii) Achieve better acceptance and efficiency, which for a study of the dimuon mass spectrum means obtaining a flatter efficiency as a function of dimuon mass. A smooth efficiency across the dimuon mass is probably fine as long as the efficiency (correction) is well understood.

The average angular deflection due to MCS of directly produced (signal) muons is given by $\theta_{\text{MCS}} \sim (Z_{\text{Target}}/p_{\mu})\sqrt{L_{\text{Target}}} \sim (1/p_{\mu}) \times (L_{\text{Target}}/\lambda_0)$. Where λ_0 is the radiation length. So to reduce the effects of MCS one should select a short target with long radiation length and use as high a beam energy as possible to produce more higher momentum signal muons.

Targets with low Z/A will have longer radiation lengths but they also have lower density and thus a longer target would be needed to get the same number of inelastic proton interactions in the target. A large signal sample needs a target with high atomic number, since the dimuon signal rate $\sim A_{\text{Target}}$. Another consideration is that the absorption probability for pions and kaons $\sim A_{\text{Target}}^{0.7}$. Thus the S/B would increase with heavier targets and dense targets. One would need to do a Monte Carlo simulation to study what target material is optimal.

If the effects of MCS can be sufficiently reduced we would need to determine the momentum of the muon more precisely. This can be achieved with a *magnetic spectrometer* where the deflection in a known magnetic field can give the magnitude of the momentum. The angle of deflection can be obtained with low mass *Multiwire Proportional Chambers (MWPC's)* placed before any of the hadron absorbers.

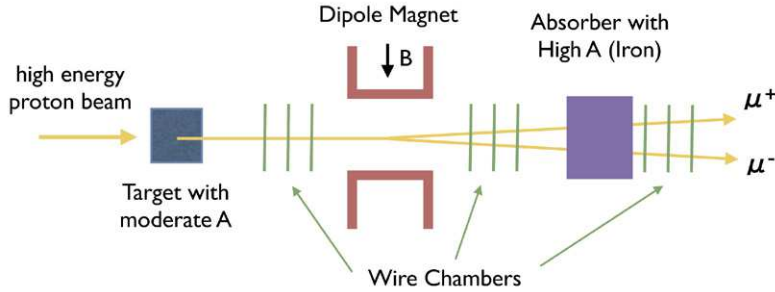


Figure 4. Schematic for one possible redesign of a detector studying dimuons where the main consideration was with improving the dimuon mass resolution.

An initial redesign of the detector might look something like the schematic in Fig. 4. However this does not have all the absorbing material of the 1970 Lederman detector to reduce background muons. For that experiment the $S/B \sim 0.04$, while in our initial design it could be as small as 10^{-6} ! To see how the S/B could be improved one has to consider the sources of background. The main ones are given below:

- (i) Direct single muons – these should be relatively small at AGS energies since the production would be through electroweak processes. Production via the decay of τ leptons or charm particles is of the same level as the J/ψ , so getting an accidental dimuon pair through these decays should cause a negligible background.

- (ii) Muons from decays of hadrons – these happen early due to an exponential decay and should therefore be absorbed early before they can decay. Also lower momentum hadrons will decay relatively sooner and thus make up a larger fraction of the decay muon background. One could try to reject softer muons from the data analysis. Also one could make multiple measurements of the momentum to reject muons from decay in flight.
- (iii) Hadrons from “punch through” – a signal in a detector element placed after an absorber can arise due to the end of a hadronic shower leaking through the absorber. One can try to detect this by having multi-absorber/detection layers which can be used to recognize a hadronic shower signal from a typically minimum ionizing muon signature. One can also try to momentum analyze through a magnetic absorber.

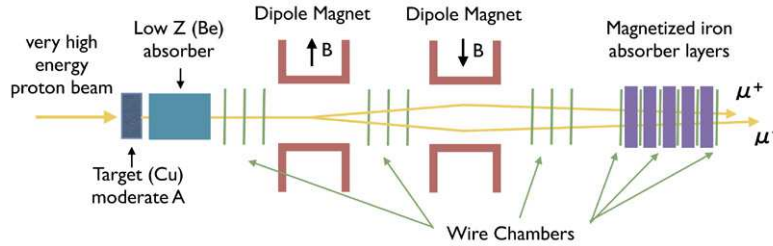


Figure 5. Schematic for a second possible redesign of a detector studying dimuons where S/B was included as a consideration as well as the dimuon mass resolution.

Another example of a revised design for the dimuon detector, this time also taking into consideration the S/B is shown in Fig. 5. It is seen that to do better than the 1970 Lederman experiment one needs a more complicated detector with considerably more advanced detectors. Even so one can see there is still a compromise made between getting the best S/B and the best dimuon mass resolution. One would need to do a serious Monte Carlo simulation to determine the optimal choices.

We have only really touched on the elements of experimental design. For example timing considerations have been completely ignored and we have assumed the wire chambers can handle the necessary rates. Instead of pursuing this further, and also before showing you Lederman’s solution, we first turn to see how Ting solves this experimental design problem.

2.3. Ting's Solution

It was recognized that the same physics could be studied by observing pairs of electrons instead of dimuons. Electrons can be produced by the same decays and have the same J^{PC} as muons, thus dielectrons should also be produced by the $J^P = 1^-$ ρ , ω , ϕ and J/ψ . However electrons differ in that they are about 200 times lighter than muons. This greatly changes the considerations for a detector designed to measure dielectron pairs compared to dimuon pairs. Although kaon and pion decays are no longer a serious source of background for a study of dielectrons, the electrons undergo much more scattering and absorption than muons. Thus the choice of materials and the detector types used to identify and track electrons is quite different.

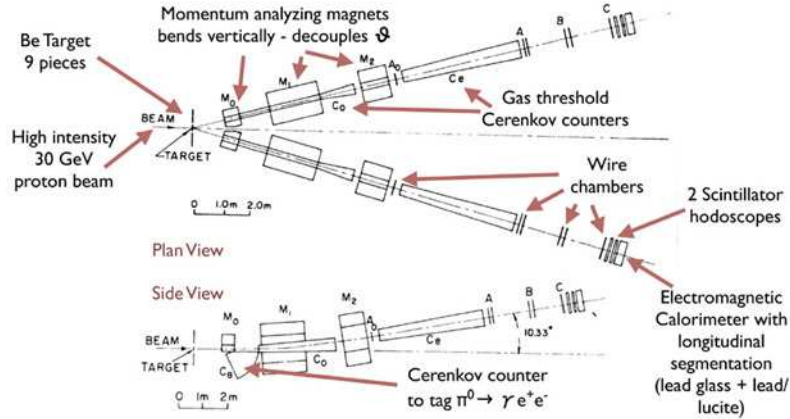


Figure 6. Schematic of the detector for Ting's J/ψ observation experiment.³

Figure 6 shows a schematic of the spectrometer used by Ting in his J/ψ observation experiment. It can be seen that the spectrometer is quite complex. Low Z beryllium targets and low mass $MWPC$'s are used to avoid too many photons converting to e^+e^- pairs. The use of a *multi-magnet spectrometer* and $MWPC$'s helped to achieve a very fine mass resolution of $\approx 5 \text{ MeV}/c^2$. Without electron identification the S/B would have been $\sim 10^{-6}$, thus a relative background rejection of 10^6 – 10^8 was needed. Typically a single particle identification detector can achieve a relative background rejection of 10^2 – 10^3 so multiple systems were combined. Both *Čerenkov counters* and *electromagnetic calorimeters* were used to identify electrons. A special *Čerenkov counter* was used to specifically reject background from

$\pi^0 \rightarrow \gamma e^+ e^-$. A relative background rejection of 10^8 was achieved and, together with a fine dielectron mass resolution, a spectacularly narrow and clean J/ψ signal was seen. The results and details of how this analysis was done are well documented in Ting's Nobel lecture³ and the published papers.⁷

2.4. *Richter's Solution*

There is another half of the J/ψ discovery story that cannot be covered in this writeup because of insufficient space. Revealed in that half would be additional important experimental techniques. For example Richter's observation of the J/ψ was made in an e^+e^- collider, a relatively new innovation at that time. A nearly 4π detector was used including *wire spark chambers* and *electromagnetic shower counters*. The J/ψ mass resolution was much better since it was governed by knowledge of the beam energy and thus the widths of states can be much better measured. That half of the story and the subsequent studies are well documented in Richter's Nobel lecture.⁴

2.5. *Improving Charmonium Spectroscopy*

An e^+e^- collider is an excellent study tool. This was recognized by Ting as well as by Richter. It is specially well suited to perform detailed studies of vector particles once their mass is known. This has been the case for charmonium, for bottomonium and for the Z^0 . Narrow states with unknown masses are difficult to find. However special modifications were made to the SPEAR e^+e^- storage ring to enable scans in energy in a relatively short time. This enabled the discovery of the J/ψ by Richter's team as well as some of the charmonium excited states. A disadvantage is that the e^+e^- collisions can only directly produce states with $J^P = 1^-$, thus only these are measured with fine resolution. While some of the non- $(J^P = 1^-)$ charmonium states could be observed through the decays of the ψ' , see Fig. 7, the measurements of their masses and widths can no longer be obtained with just the knowledge of the beam energies.

Further improvement in the knowledge of the charmonium spectrum has been achieved by using low energy $p\bar{p}$ collisions in an antiproton accumulator. The first of these experiments was done at the CERN ISR in R704, then in E760 and E835 at the Fermilab antiproton accumulator.⁸ In the Fermilab experiments, a hydrogen gas-jet target is used and the antiproton beam is tuned to produce and precisely measure charmonium states of any

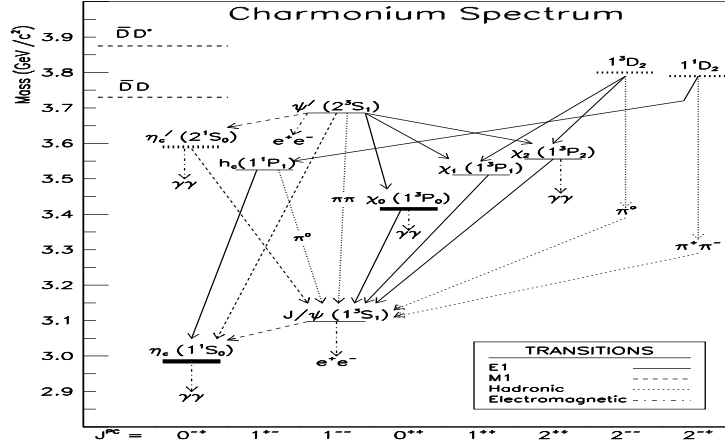


Figure 7. Schematic of the charmonium energy levels.

J^P . The charmonium states are tagged by their electromagnetic decays using *lead glass shower counters* and *scintillating fibres*. All that is needed is to recognize signal from background. The actual mass and width measurements is determined with exquisite ($\sim 0.01\%$) resolution due to excellent knowledge of the beam energy.

2.6. Lederman's Two Solutions

We conclude the first part of the mini-course with two of Lederman's solutions to the dilepton experiment design problem. The first is his 1976 experiment that looked at e^+e^- pairs using a higher energy beam running at Fermilab.⁹ This detector was a relatively simple experiment using a *magnetic spectrometer* for momentum determination and a *lead-glass calorimeter* for electron identification. Although the J/ψ was clearly visible in this experiment, the background was still relatively high. A cluster of events was observed at $M_{e^+e^-} \approx 6 \text{ GeV}/c^2$ which lead to a claim of a possible observation of a narrow peak at this mass. What was observed was most likely a background fluctuation.⁶ Lederman's second solution was a 1977 experiment to look at dimuons using a far more complicated detector and again running at Fermilab.¹⁰ This was a far more successful experiment in which the first observation of the Υ was made, the first indication of a new fifth quark. Unfortunately observations of new quarks were apparently no longer deemed worthy of a Nobel prize by this time. However the reader

need not feel too bad for Leon Lederman since he was awarded the Nobel prize anyway in 1988, sharing it with Melvin Schwartz and Jack Steinberger for their use of neutrino beams and discovering a second type of neutrino, the muon neutrino.¹¹

3. Part II: More on Charm and Bottom Quarks

In Part I the discovery of charm was used to introduce some basic detectors components. *Scintillators, Photomultiplier Tubes, wire chambers, magnetic spectrometers, Čerenkov counters*, and *electromagnetic calorimeters* were mentioned. In Part II additional experimental topics are covered, namely the following: particle identification systems; the use of precision position detectors to observe detached vertices; the use of different beam types; and the evolution of trigger systems. The story for this part of the mini-course is the advancement of detection of particles containing charm and bottom quarks. The outline of this part is illustrated in the bottom section of Fig. 1.

3.1. Open Charm Discovery

In Sec. 2 we introduced the discovery of the charmonium ($c\bar{c}$) states where the charm quantum number is hidden. The charm quark explanation of the observed narrow states became universally accepted once states with open charm were discovered.

The two most commonly produced charm mesons are the D^0 ($c\bar{u}$) and the D^+ ($c\bar{d}$). The charm quark decays quickly to either a strange quark or a down quark. The ratio of the rates for these two decays is given by the ratio of the square of two CKM matrix elements: $\Gamma(c \rightarrow sW^*)/\Gamma(c \rightarrow dW^*) \sim |V_{cs}|^2/|V_{cd}|^2 \approx 20$. The $c \rightarrow sW^*$ decay is called Cabibbo favoured while the $c \rightarrow dW^*$ is Cabibbo suppressed. The virtual W can decay to either quarks or leptons. Thus most of the D^0 and D^+ mesons decay to states with a strange quark. The easiest decay modes to reconstruct are the all charged modes: $D^+ \rightarrow K^- \pi^+ \pi^+$; $D^0 \rightarrow K^- \pi^+$; and $D^0 \rightarrow K^- \pi^+ \pi^+ \pi^-$. Since pions are the more copiously produced hadrons in an interaction, one needs to distinguish kaons from pions to observe these open charm signals.

Besides *Čerenkov counters* there are other particle identification methods for charged hadrons. One example is a *Time-of-Flight (TOF)* detector, this was used in the discovery of open charm two years after the discovery of the J/ψ . The discovery was made using the Mark I experiment at the SPEAR e^+e^- collider, the same spectrometer which was used in the dis-

covery of the J/ψ . The e^+e^- collider gives an inherently lower background than hadron-hadron collisions since the electron and positron annihilate completely. However the $D^+ \rightarrow K^- \pi^+ \pi^+$ and $D^0 \rightarrow K^- \pi^+$, $K^- \pi^+ \pi^+ \pi^-$ were only discovered after the collection of additional data and using the TOF system to separate kaons from pions.

A TOF system works by measuring the time it takes for a charged particle to travel between two points. For particles of the same momentum, this time difference depends on the particle's mass.

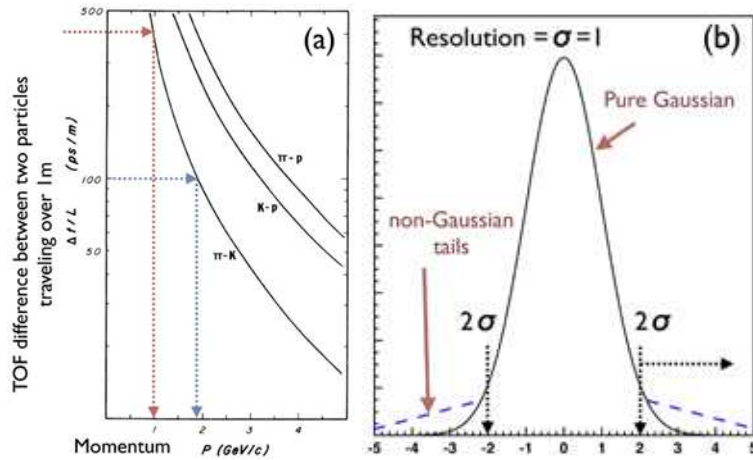


Figure 8. (a) Time-of-flight differences for pairs of particles plotted against momentum; (b) Illustration of a Gaussian resolution function and example of non-Gaussian tails.

Figure 8(a) shows the difference in time-of-flight over one metre for pairs of hadrons. The performance of a TOF system is given by the distance (L) traveled between the two time measurements and the resolution ($\sigma_{\Delta t}$) with which the time-of-flight measurement is made. Long distances and fine resolution are needed. For example for Mark I $L \approx 2$ m and $\sigma_{\Delta t} \approx 400$ ps. This means that one can get $2\sigma_{\Delta t}$ separation between kaons and pions for momenta < 1 GeV/c, *i.e.* at very low momentum. Even if the time measurement resolution can be considerably reduced, *e.g.* to ≈ 100 ps for the Fermilab CDF Run II experiment, it can be seen from Fig. 8(a) that with $L \approx 2$ m, a $2\sigma_{\Delta t}$ separation between kaons and pions is only achieved for momenta < 2 GeV/c. Even with only a $2\sigma_{\Delta t}$ separation at low momentum, the decays $D^0 \rightarrow K^- \pi^+$, $D^0 \rightarrow K^- \pi^+ \pi^+ \pi^-$ and $D^+ \rightarrow K^- \pi^+ \pi^+$ could be isolated sufficiently from background at Mark I for them

to make the discovery.¹² The mass plots are shown in Fig. 9, the $D^0 \rightarrow K^- \pi^+$ distribution is shown without and with a *TOF* kaon selection.

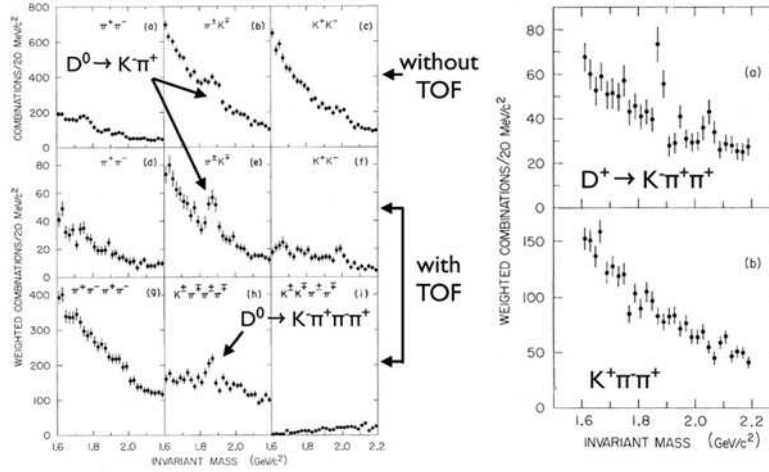


Figure 9. Mass plots from Mark I: (Left) D^0 ; (right) D^+ .

The gas *Čerenkov counters* mentioned in Part I can be used to separate kaons and pions at higher momenta, but typically collider experiments like Mark I and CDF do not have the necessary space for them. There are a number of alternate particle identification systems.¹

3.2. Measurement Uncertainties

At this point it is worth making an aside about experimental resolution and the meaning of a $2\sigma_{\Delta t}$ separation. The importance of mass resolution was introduced in Sec. 2.1. Not only is the size of the resolution important, but the resolution function or shape matters also. When a quantity is measured experimentally one does not typically obtain an exact number, but there is some uncertainty. This uncertainty is normally separated into two components. One component is essentially statistical in nature and arise due to a lack of precision. The other is typically non-statistical and is due to our limited knowledge and affects the accuracy of the measurement. The former is called the statistical uncertainty or statistical error, while the latter is referred to as the systematic uncertainty.

A classic example of a statistical uncertainty is that due to limited statistics. *E.g.* when measuring the lifetime of a particle we have a limited

number of particles to use, thus the lifetime distribution is measured with limited precision which leads to an uncertainty in the extracted lifetime. Another example is measuring a distance with a measuring tape. There is some uncertainty in positioning the tape at one end and in the reading and the precision of the scale at the other end. To reduce this uncertainty the measurement can be repeated many times and the average value used. We can illustrate the resolution with this simple example. If a histogram is made of these measurements (frequency *vs.* [value–nominal]) ideally the distribution is Gaussian as shown by the solid line in Fig. 8(b). The resolution is the sigma of the Gaussian distribution, and it gives the statistical uncertainty of any single measurement.

Imagine Fig. 8(b) shows the distribution of time-of-flight measurements for pions, where the nominal value is subtracted off and normalized to the resolution $((\Delta t - \Delta t_0)/\sigma_{\Delta t})$. For any given pion the Δt measured can fall anywhere within the Gaussian distribution. In particular for a small fraction of the time it could be larger than $2\sigma_{\Delta t}$ from nominal, for a Gaussian distribution this probability is about 3%. Suppose that for a kaon the measured value of $(\Delta t - \Delta t_0)$ is greater than $2\sigma_{\Delta t}$. Then by requiring $(\Delta t - \Delta t_0) > 2\sigma_{\Delta t}$ we can select kaons and reject 97% of pions. This is for an ideal Gaussian distribution. The resolution function typically has non-Gaussian tails that go out much further as illustrated crudely by the dashed lines in Fig. 8(b). The rejection in this case would not be as good as 97%. Thus one needs to know the resolution function and must take care to try to avoid large non-Gaussian tails. For a real *TOF* system, non-Gaussian tails could arise from a number of sources, and the tails could also be asymmetric. Some of these sources include the following.

- The counter giving the time signal is finite in size and the measurement will depend on where the particle hits the counter.
- The system is made up of many counters whose relative timing and locations are not perfect.
- The calibration is not perfect, *e.g.* calibration tracks do not always come from exactly the same point, and the start time is not perfectly known.
- Some effects like MCS may affect the resolution and cause it to vary with the particle momentum.

Further coverage of statistical uncertainties and how to determine and handle them are beyond the scope of this mini-course, but there are many excellent books on this subject.¹³

The other component of a measurement uncertainty is called the systematic uncertainty and it is typically not statistical in nature. A classic example can again be illustrated by the case of measuring a distance with a measuring tape. If the scale of the measuring tape is wrong we would get a systematic error. Of course, if it were known that the scale was incorrect, we would correct the scale and the systematic error would be eliminated. Now let us assume that we must calibrate the measuring tape ourselves. We can only calibrate the scale within a certain accuracy, and this leads to a systematic uncertainty in the distance measured. For a more realistic example consider measuring the lifetime of a decaying particle. For a short lived particle like the D^0 , the time is not directly measured. Instead, the distance (L) traveled between production and decay is measured and the momentum of the particle is also measured. The proper time for the decay is then $t = Lm_{D^0}/p_{D^0}$. Besides the length and momentum scales, there are other potential sources of systematic uncertainties. The lifetime is extracted from a lifetime distribution containing many particle decays. This distribution may not be a pure exponential but could be modified due to detector acceptance and efficiency. The correction for acceptance and efficiency is typically determined using a Monte Carlo simulation. There are inherent uncertainties in the simulation that lead to an uncertainty in the correction function and thus to a systematic uncertainty in the lifetime. If the particle passes through matter before decaying or the daughter particles pass through matter, the lifetime distribution can also be affected by absorption of the parent or daughter particles. The cross sections for absorption may be poorly measured or not even known. This limited knowledge can also lead to a systematic uncertainty in the measurement. Finally, another source of systematic uncertainty could be backgrounds that mimic the signal but which are not properly accounted for. Typically, systematic uncertainties are not well defined and are not straightforward to determine. They are also usually not Gaussian distributed, and combining systematic uncertainties from different sources is problematic. Since even the meaning and definition of systematic uncertainties are difficult to quantify, ideally one should design an experiment to have a small systematic uncertainty (compared to the statistical uncertainty), so as not to have to worry about the details of the treatment and combining of systematic uncertainties. Further coverage of systematic uncertainties is beyond the scope of this mini-course. The understanding of systematics is beginning to be better understood and in some rare cases are even correctly taught.¹⁴ However considerable disagreements are still common.

3.3. Improving S/B for Open Charm

Although the use of particle identification can be powerful in isolating a signal, it can be seen from Fig. 9 that there is considerable room for improvement. This is especially true in hadronic interactions which typically have higher backgrounds than in e^+e^- annihilations.

The lifetimes of the open charm particles are in the range 0.1–1 ps, which is small but finite and can be used to isolate a signal. Almost all the u - and d -quark backgrounds have essentially zero lifetime while the backgrounds from some strange particles decay after a long distance. Thus the signature of a charm particle is given by its decay a short distance away from the production point. For example, a 30 GeV D^0 travels an average length of about 2 mm, which is quite small but increases linearly with momentum.

To get a better sense of the scale involved, consider the decay of a charm particle produced in a fixed-target experiment as illustrated in Fig. 10(a). The charm particle is produced and then decays after traveling a distance L_D . To separate the production and decay vertices we need to measure L_D with a resolution of $\sigma_{L_D} \ll L_D$. Since position detectors typically measure in the dimension transverse to the beam direction, it is more convenient to transform this essentially longitudinal resolution requirement into an transverse one. The typical angle that the charm particle is produced relative to the beam direction is $\theta \approx m_D/p_D$, where m_D and p_D are the mass and momentum of the charm particle respectively. The mean distance traveled by the charm particle is $L_D = \beta\gamma c\tau_D = c\tau_D p_D/m_D$ where τ_D is the lifetime of the charm particle. Thus to resolve the production and decay vertices we need $\sigma_{trans} \ll \theta L_D$, or $\sigma_{trans} \ll c\tau_D$, where σ_{trans} is the transverse position resolution of the detector (charged) tracking system. The values of $c\tau_D$ for the D^0 , D^+ and Λ_c^+ are 123 μm , 312 μm and 60 μm respectively.

The resolution of the $MWPC$'s depend on the wire spacing (s), and for a single detector plane is given by $\sigma_{trans} = s/\sqrt{12}$. The minimum wire spacings are in the range 1–2 mm depending on their cross sectional coverage. For $s = 2$ mm, $\sigma_{trans} = 577 \mu\text{m}$, too large to resolve the production and decay vertices. The spatial resolution can be improved by measuring the time between a charged particle passing through the detector plane and when a signal is received in the wire closest to the point of passage. This is done in *Drift Chambers* and resolutions as low as $\sigma_{trans} \approx 100 \mu\text{m}$ have been obtained in such a tracking system. This is still too large, especially considering that one typically needs better than 5–10 σ vertex separation.

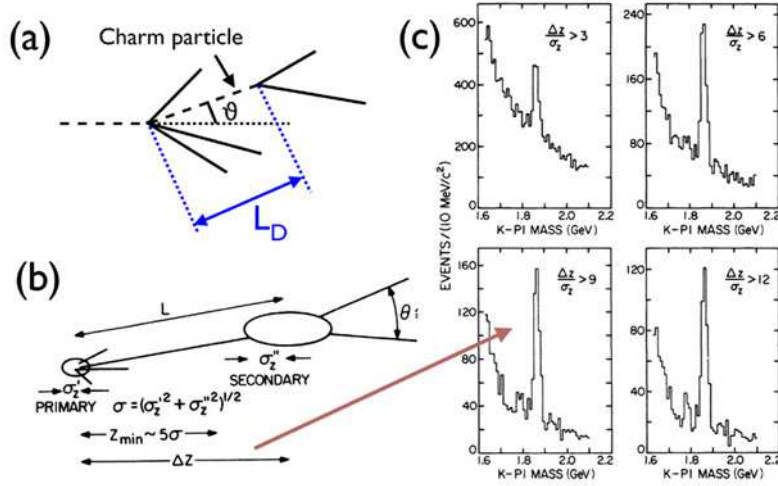


Figure 10. (a),(b) Illustration of production and decay of a charm particle. (c) Invariant $K-\pi^+$ mass plots from E691 showing the power of a detached vertex requirement.

A tracking system with much better spatial resolution is needed. Historically, two detector technologies have been used that can give better resolutions: *photographic emulsions* and *Bubble Chambers*.

Detection using layers of photographic emulsions has been used for a long time and spatial resolutions of better than $10 \mu\text{m}$ have been obtained. Although these have been used relatively recently in DONUT to make the first direct observation of the ν_τ ,¹⁵ they are not suitable for high rates.

Bubble Chambers have also been used historically to make important observations. Typically, the resolution of bubble chambers is not better than that for *Drift Chambers*. However, a sufficiently small bubble chamber, like the LEBC in the LEBC-EHS experiment, has achieved resolutions of $\sim 10 \mu\text{m}$, but again such bubble chambers are not suitable for high rates. The LEBC-EHS experiment reconstructed about 300-500 charm decays.¹⁶

What launched the high statistics studies of charm quark physics was the development and use of the *Silicon Microstrip Detector (SMD)*. The Fermilab E691 photoproduction experiment included one of the first *SMD*'s and collected a 10,000 sample of fully reconstructed charm decays, about two orders of magnitude more than other experiments of that time. Resolutions as good as $\sigma_{trans} \sim 10 \mu\text{m}$ can be obtained and some data from E691 are shown in Fig. 10(c).¹⁷ *SMD*'s have now been used in many experiments including those studying bottom and top quarks.

3.4. Going for Higher Statistics

The road to higher statistics in charm studies is illustrated in Fig. 11, giving some selected milestones along the route.

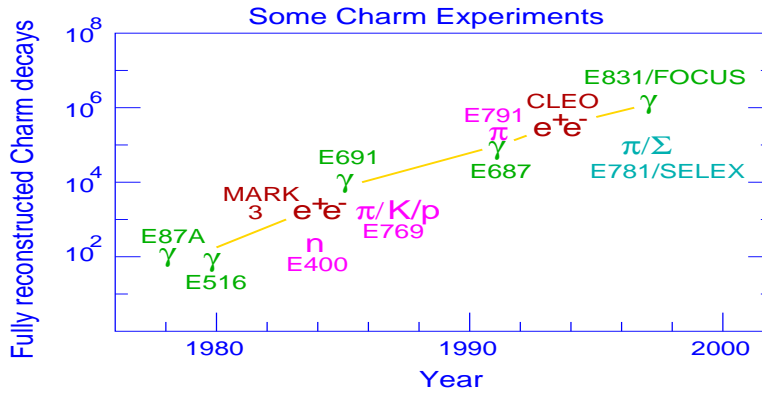


Figure 11. Number of fully reconstructed charm decays for different experiments as a function of time.

The charm quark experiments include e^+e^- and $p\bar{p}$ colliders as well as fixed-target experiments using photon and hadron beams. While larger charm data sets could be obtained in e^+e^- experiments by increasing the luminosity (*e.g.* CLEO), the fixed-target experiments needed additional technological advances – the 8 mm tape for data storage and high power commodity computing for data processing. For example, using these technologies and by building a more intense photon beam, the Fermilab FOCUS photoproduction experiment obtained a sample of 1 million fully reconstructed charm decays with published physics results one year after the end of data taking. Using 8 mm tapes with 30 times the capacity of 9-track tapes, the Fermilab E791 hadroproduction experiment could write out much more data and collected more charm than previous hadroproduction experiments. To do this, E791 used a wall of 42 8 mm tape drives in parallel to record data fast enough. To obtain substantially more statistics, a revolution in triggering is needed.

3.5. The Trigger System and the Bottom Quark

Typically the particle interactions occur at a high rate and the S/B can be as low as 10^{-3} – 10^{-8} . A trigger system is used to quickly decide whether an

interaction contains signal and thus “trigger” the recording of the related data.

For a charm photoproduction experiment like FOCUS, the photon beam largely produces e^+e^- conversion pairs and only about 1 in every 500 photon interactions would produce hadrons. Only 1 in every 150 of those interactions producing hadrons contains a charm quark. It is relatively easy to recognize a photon conversion from an interaction producing hadrons. Since the fraction of hadron producing interactions containing charm is not too small, one just writes out all hadron producing interactions. For hadroproduction experiments on-the-other-hand, the fraction of charm is smaller by another factor of ten, thus either a lot more data must be written out and analyzed or a better, more intelligent trigger must be used.

Historically the trigger is a system of fast electronics that quickly processes special trigger signals produced by the detector and gives an electronic acceptance decision that is used to “trigger” the readout to save the data for that interaction. Long cables are used to delay the signals from the rest of the detector so they do not arrive at the readout before the trigger decision is made. In addition, the experiment is “dead” and unavailable to collect more data until the data readout is completed – this dead-time can be a significant fraction of the live-time. In the first stage of the FOCUS trigger, the decision must be made within about 370 ns from the time the interaction occurs.

Developments have made modern trigger systems much easier. Electronics are now faster, smaller and cheaper. Also, high speed data links and computing resources are more powerful. A large amount of memory is now affordable so that data from the detectors can be stored digitally while the trigger processing takes place. This eliminates the need for long signal cables which can degrade analog signals, and it also gives more time for trigger processing and virtually eliminates dead-time.

The ultimate trigger is if all the data could be recorded and analyzed before deciding which data to store. One can illustrate what is needed for such a trigger by using as an example the CDF or D0 experiments at Fermilab. In these experiments, protons and antiprotons cross every 396 ns, so there are about 2.5×10^6 crossing/s. If it took one second to fully analyze the data from one crossing in a single CPU, we would need 2.5 million CPU's to not lose data from any crossings. We would also need to temporarily store at least 2.5 million crossings worth of data. If one needs 300 KB/crossing, then 1 TB (10^3 GB) is needed. Since the processing time would have a long tail beyond one second, to be safe one would want about

1000 TB of RAM as well as the 2.5 million CPU's! Clearly a trigger that only partially processes the data is needed.

Even if the ultimate trigger cannot yet be realized, the developments mentioned above have provided the needed ingredients to separate out charm decays in hadronic collisions by looking for evidence of a detached decay vertex at the trigger level. Since recognizing bottom quark decays is similar to that for charm decays, this revolution in triggering has made possible an experiment that will reconstruct very large samples of charm and bottom decays.

Already large samples of charm and bottom quark decays are being collected using the BaBar and Belle e^+e^- experiments. To do better one must use hadronic collisions with sufficient energy like $p\bar{p}$ annihilations at the Fermilab Tevatron. The cross section for producing bottom quarks is much larger than in e^+e^- annihilations, *e.g.* about $100 \mu\text{b}$ compared to about 1.1 nb at the $\Upsilon(4S)$. The CDF and D0 $p\bar{p}$ experiments can collect sizable samples of charm and bottom decays, but to get 1000 times more rate than BaBar or Belle requires a specialized detector and data acquisition and trigger systems.

The BTeV experiment¹⁸ is designed to study bottom and charm decays at the Tevatron. To maximize the yield for clean flavour-tagged B mesons for CP violation studies, the detector is placed in the forward direction allowing a *Ring Imaging Čerenkov Counter (RICH)* for excellent particle identification over a wide momentum range. A PbWO_4 crystal calorimeter provides efficient detection of photons and π^0 's with excellent energy resolution. The BTeV experiment includes a *silicon pixel detector* that makes possible the recognition of detached vertices at the lowest trigger level.

Although a *SMD* can provide excellent spatial resolution, a lot of data processing is typically needed for interactions with many tracks due to the strip geometry. This is illustrated in Fig. 12(a). A single particle passing through a plane of strips will give a signal in one strip as illustrated in (i). The location along the hit strip can be determined by a second plane of strips oriented at 90° to the first plane as in (ii). However if, as illustrated in (iii), two particles pass through the two planes we would get four hit strips and one cannot tell if the two particles passed through points (A1, A2) or through (B1, B2). This ambiguity may be resolved by a third plane of strips at an angle as given in (iv). For a complex event with many particles the pattern recognition becomes quite complex and requires significant CPU power.

Ideally a trigger algorithm should be close to that used in the data

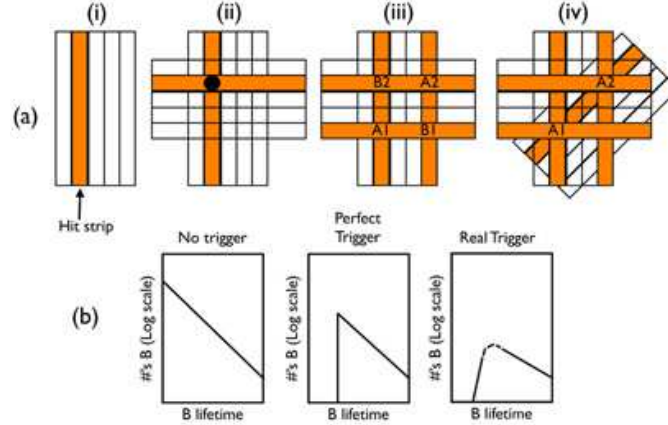


Figure 12. (a) Illustration of pattern recognition in a *SMD*. (b) Illustration of the effect on the lifetime distribution of a detached vertex trigger.

analysis but with looser selection criteria. This is because a poorly chosen trigger algorithm can give rise to sizable systematic uncertainties. A simple example is illustrated in Fig. 12(b). The lifetime distribution of the B^0 meson is shown which is a pure exponential with the B^0 lifetime. Since backgrounds are typically at low lifetimes, an ideal trigger for collecting data to measure the lifetime would select decays with a large enough lifetime as illustrated in the middle distribution of Fig. 12(b). In a real trigger there is typically only time to do partial processing, and thus one might require only the presence of one or two detached tracks, instead of reconstructing the production and B^0 decay vertices. This could lead to a lifetime distribution illustrated by the right-most distribution of Fig. 12(b). Thus a correction function is needed to extract the correct B^0 lifetime.

The charged track pattern recognition is simplified in BTeV by the use of $400 \times 50 \mu\text{m}^2$ *silicon pixels* which can locate the position of a passing particle in 3-dimensions by a single hit pixel. Low momentum tracks undergo more MCS and can give rise to false detached tracks. In BTeV, the pixel detector is located in a dipole magnet so that tracks with low momentum can be rejected and not used at the trigger level.

Even with *silicon pixels* a full reconstruction cannot be done. Custom electronics using 500 FPGA's are used to help in processing the 500 GB/s data rate coming from the detectors. Further data processing and the pattern recognition is done on 500 commercial IBM-G5-equivalent processors. Two further levels of the trigger running on 1500 commodity CPU's reduce

the data going to storage to a more manageable 200 MB/s.

The BTeV experiment nicely illustrates the convergence of a number of technological advances. Years of scientific progress have enabled such an experiment to be realized.

Glossary

Bubble chamber: A historic detector consisting of a liquid maintained at a pressure above the equilibrium vapour pressure. The bubble chamber can be expanded to suddenly decrease the pressure so that charged particles passing through the liquid in a “superheated” condition will create a track of bubbles. Photographs are taken of the bubbles in multiple views to reconstruct the particle trajectories.

Calorimeter: A device to measure the energy of particles. The two distinct types are *electromagnetic calorimeters* and *hadronic calorimeters*. They work by completely absorbing the shower produced by a particle and producing a signal proportional to its energy. Calorimeters must be calibrated to give the absolute particle energy.

Čerenkov counter: A detector based on the Čerenkov effect (for which Čerenkov shared the 1958 Nobel prize). Particles traveling faster than light in a given medium emits a cone of (Čerenkov) light. A threshold Čerenkov counter contains a gas, for example, with a well chosen refractive index so that for a given particle momentum one particle type (*e.g.* pions) will emit light while another (*e.g.* kaons) will not. The angle of the cone of light also depends on the particle velocity which is used in other forms of *Čerenkov counters* like the *RICH*. The amount of Čerenkov light emitted is typically low, about 100 times less intense than scintillation light in a scintillator.

Drift chamber: A *wire chamber* where one measures the time between when a charged particle passes through and when a signal in the nearest signal wire is received. Typically many wires are used to form drift cells where the electric field is tailored to obtain a fairly uniform drift velocity across the cell. The spatial resolution is better than a *MWPC* but a drift chamber is more complex and typically cannot handle as high a rate of particles.

Electromagnetic calorimeter: A *calorimeter* for measuring the energies of photons and e^\pm through their electromagnetic interactions. These calorimeters can be made from dense crystals like PbWO_4 or *lead-glass*, or

can be sandwiches made of multiple layers of dense absorber and detection material.

Emulsions: Usually a layer of photographic emulsion several hundred μm thick in which a traversing charged particle causes the nearest silver halide grains to develop. Each grain is typically $0.2 \mu\text{m}$ in diameter with about 270 developed grains/mm. The emulsion must be scanned to reconstruct the particle trajectories.

Lead-glass shower counters: A dense glass used to detect photons and e^\pm and for *electromagnetic calorimeters*. The detection is based on Čerenkov light.

Magnetic Spectrometer: A detector system used to determine the momentum of charged particles by measuring the deflection of the particles in a known magnetic field. Various magnetic field configurations can be used *e.g.* dipole, solenoid, or toroid. Deflection of particles are measured using position detectors, usually *wire chambers*, but can be *e.g.* *scintillator hodoscopes*, *scintillating fibres* or a *SMD*.

Multiwire proportional chamber (MWPC): A *wire chamber* where the location of a passing charged particle is determined by the location of the wire closest to it.

Photomultiplier Tube (PMT): A device to detect a small quantity of light using the photoelectric effect (for which Einstein received the 1921 Nobel prize). The maximum sensitivity of the photocathode in a typical *PMT* is for blue light.

Ring imaging Čerenkov counter (RICH): A Čerenkov counter where the angle of the emitted Čerenkov light is measured to enable the identification of particles over a wide momentum range.

Scintillator: A material that produces light through fluorescence when a charged particle passes through it. Scintillators used include inorganic crystals like PbWO_4 , organic liquids and plastic. A classic plastic scintillator is made of polystyrene that produces light in the UV. The UV light is shifted to blue with a tiny doping of primary and secondary fluors to better match the photosensitivity of a *PMT*. Most of the light comes in a fast component (few ns) and strong signals are possible with sufficient scintillator thickness.

Scintillator fibres: *Scintillator* in the form of long flexible fibres with an outer acrylic sleeve so that the scintillation light is isolated to the fibre, but still totally internally reflected along the fibre to the ends. Typically a few mm in diameter they are used for position detectors or in *calorimeters* as either the detection material or as a mechanism for readout.

Scintillator hodoscope: A single detector plane made of strips of *scintillator*. Used to detect the position of a charge particle. Two planes can be overlapped with the strips in one plane oriented at 90° to the other to locate the particle in both transverse dimensions.

Silicon microstrip detector (SMD): Detection is based on essentially a silicon semiconductor p-n junction where the depletion region is enlarged by a bias voltage. The depletion layer can be considered as a solid state ionization chamber. A charged particle passing through the depletion region liberates electron-hole pairs which create signals on very thin, closely spaced readout strips. *SMD*'s have the detection regions arranged as long uniformly separated strips. The strip separation can be in the range 10–300 μm .

Silicon pixels: Similar to the *SMD* but the active region is in the form of rectangles so that a “hit” pixel locates a passing particle in both transverse dimensions. The readout is however more complicated.

Spark wire chamber: A parallel-plate gas chamber in which a high voltage pulse is applied immediately after the passage of a passing charged particle. Sparks form along the trail of ions caused by the charged particle passing through the gas. This can provide a visualization of the track useful for public demonstration. High speed readout is typically done magnetostriictively or capacitively.

Time-of-flight detector: A system for identifying charged particles based on measuring their velocity between two points. The time-of-flight between two points is usually measured using *scintillator* counters possibly in conjunction with a measurement of the time of an interaction. The particle momentum is also measured giving a velocity that can distinguish particle types through their differing masses. See Sec. 3.1.

Wire chamber: For detection of charged particles through their ionization of usually noble gas atoms. A high voltage causes ionized electrons to accelerate and create an avalanche of electrons and positive ions. Detection of the avalanches in a plane of wires can give the position of the passing

particle. Many types of wire chambers have been used, the original type (*MWPC*) was invented by Charpak for which he received the 1992 Nobel prize.

Acknowledgments

My thanks to Jeff Appel for some helpful suggestions for these lectures and for a careful reading of this writeup. This work was supported by the Universities Research Association Inc. under Contract No. DE-AC02-76CH03000 with the U. S. Department of Energy.

References

1. Some examples of textbooks are: R. Fernow, *Introduction to experimental particle physics*, CUP 1986; K. Kleinknecht, *Detectors for particle radiation*, 2nd Ed., CUP 1998. There are also some excellent articles, *e.g.* in F. Sauli (Ed.), *Instrumentation in High Energy Physics*, World Scientific, 1992.
2. R. N. Cahn and G. Goldhaber, *The experimental foundations of particle physics*, CUP 1989.
3. S. C. C. Ting, Nobel Lecture, 11 Dec. 1976, the full text is available at <http://nobelprize.org/physics/laureates/1976/ting-lecture.pdf>.
4. B. Richter, Nobel Lecture, 11 Dec. 1976, the full text is available at <http://nobelprize.org/physics/laureates/1976/richter-lecture.pdf>.
5. J. H. Christenson *et al.*, *Phys. Rev. Lett.* **21**, 1523 (1970).
6. L. M. Lederman, Nobel Lecture, 8 Dec. 1988, the full text is available at <http://nobelprize.org/physics/laureates/1988/lederman-lecture.pdf>.
7. J. J. Aubert *et al.*, *Phys. Rev. Lett.* **33**, 1404 (1974); *Nucl. Phys.* **B89**, 1 (1975).
8. M. Ambrogiani *et al.*, *Phys. Rev.* **D64**, 052003 (2001).
9. D. C. Horn *et al.*, *Phys. Rev. Lett.* **36**, 1236 (1976).
10. S. W. Herb *et al.*, *Phys. Rev. Lett.* **39**, 252 (1977).
11. G. Danby *et al.*, *Phys. Rev. Lett.* **9**, 36 (1962). See also the Nobel lectures at <http://nobelprize.org/physics/laureates/1988/>
12. G. Goldhaber *et al.*, *Phys. Rev. Lett.* **37**, 255 (1976); I. Peruzzi *et al.*, *Phys. Rev. Lett.* **37**, 569 (1976).
13. Some examples of statistics textbooks are: P. R. Bevington and D. K. Robinson, "Data Reduction and Error Analysis for the Physical Sciences", 2nd Ed., McGraw-Hill 1992; G. Cowan, "Statistical Data Analysis", OUP 1998; D. S. Sivia, "Data Analysis: A Bayesian Tutorial", OUP 1996.
14. R. Barlow, "Systematic Errors: Facts and Fictions", hep-ex/0207026.
15. K. Kodama *et al.*, *Phys. Lett.* **B504**, 218 (2001).
16. M. Aguilar-Benitez *et al.*, *Z. Phys.* **C40**, 321 (1988).
17. J. C. Anjos *et al.*, *Phys. Rev. Lett.* **58**, 311 (1987); K. Sliwa *et al.*, *Phys. Rev.* **D 32**, 1053 (1985); J. R. Rabb *et al.*, *Phys. Rev.* **D 37**, 2391 (1988).
18. <http://www-btev.fnal.gov/>